# Supporting Information

## Enhancing plasmonic hot carrier generation by strong coupling of multiple resonant modes

*Yat Lam Wong, Huaping Jia, Aoqun Jian, Dangyuan Lei*, Abdel I. El Abed, and Xuming Zhang**

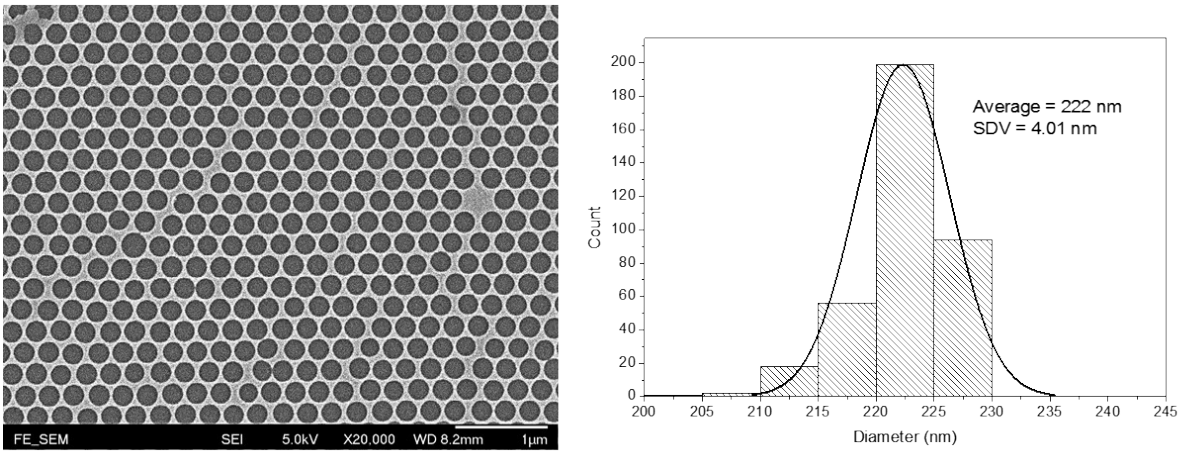


Fig. S1. The SEM image (left) and the distribution of the diameter of holes (right) extracted from the SEM image. The average and standard deviation of the holes‘ diamter are 222 nm and 4.01 nm, respectively.

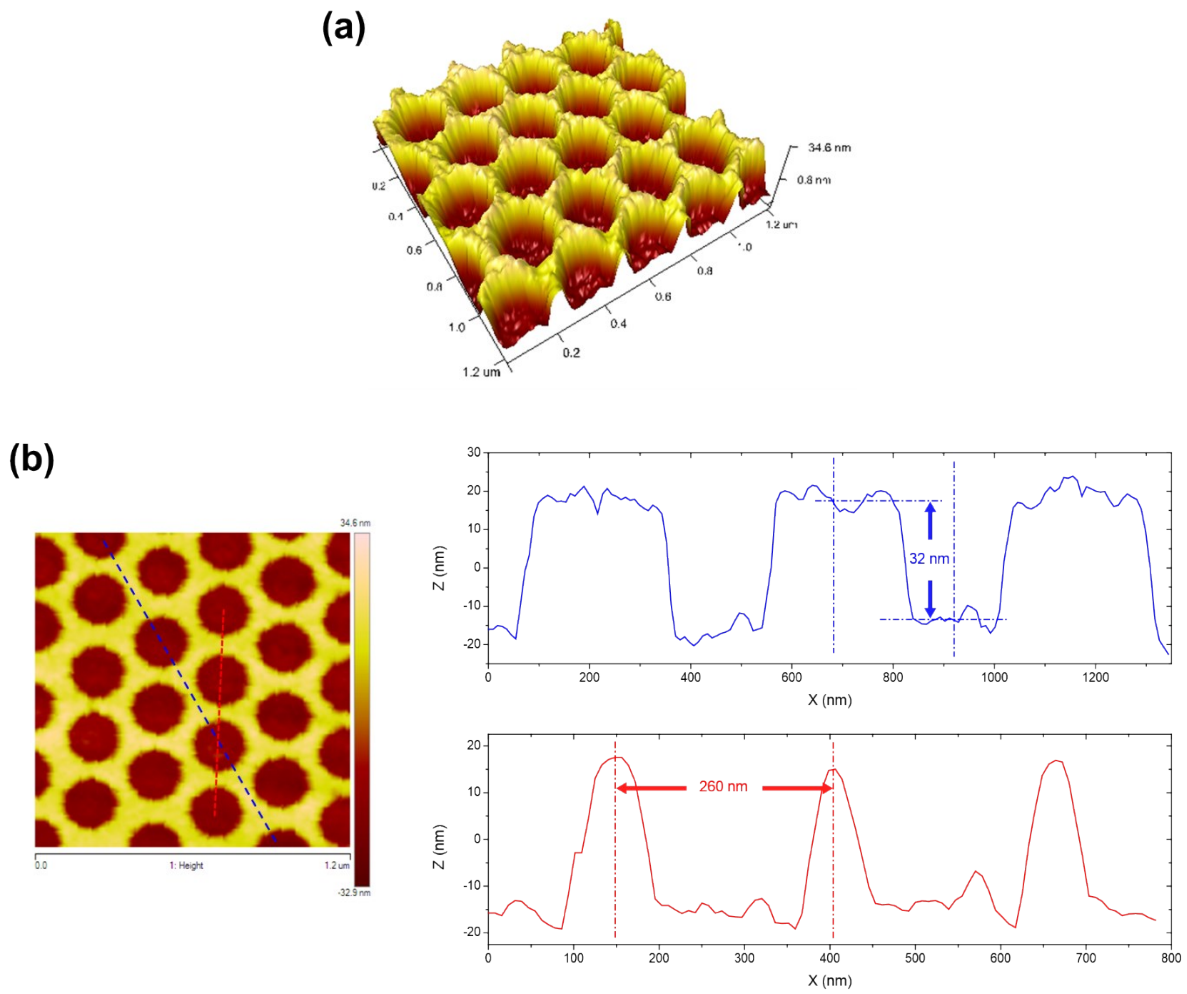


Fig. S2. The 3D AFM image of the AuNHA (a); and the top view and the profiles of along the blue and red dash lines (b).

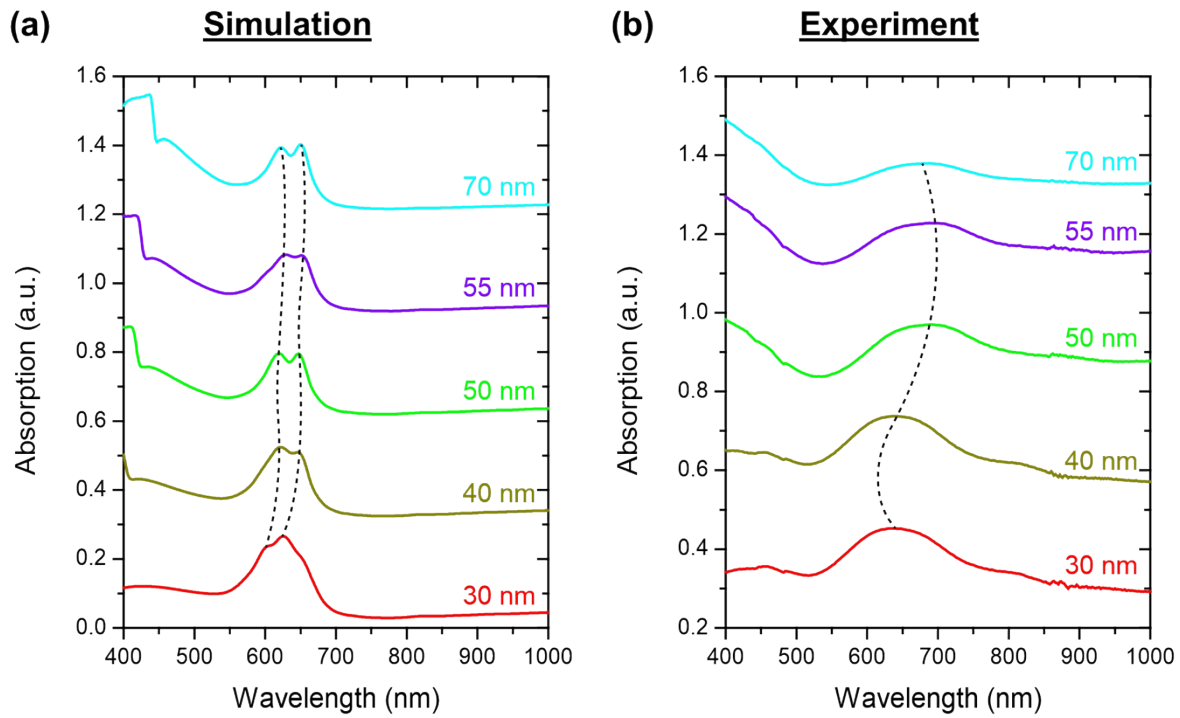


Fig. S3. The FDTD calculated (a) and experimental (b) absorption spectra of the AuNHA/$TiO_2$ metal-dielectric (MD) absorbers with the $TiO_2$ thicknesses of 30, 40, 50, 55, and 70 nm (from bottom to top).

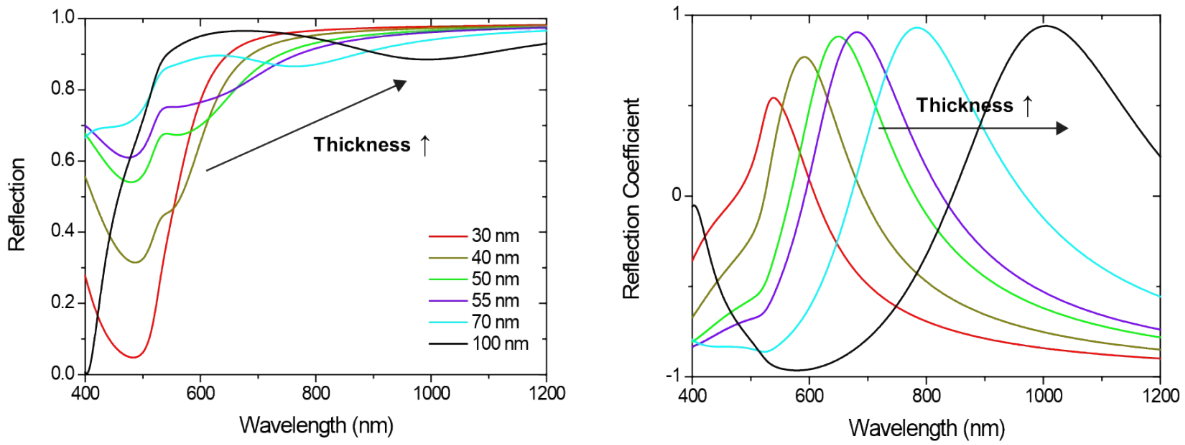


Fig. S4. The reflection spectra (left) and the associated reflection coefficient (right) of the $TiO_2$/Au/$SiO_2$ structure with different $TiO_2$ thicknesses.

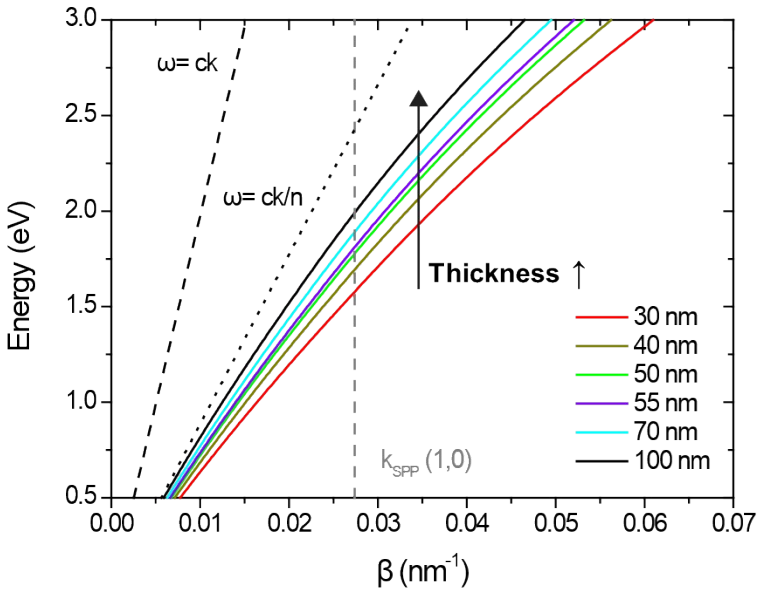


Fig. S5. The dispersion relation of the GSPP mode supported by the AuNHA/$TiO_2$/Au MDM structure with different thicknesses of $TiO_2$ layer. The black dashed line and the black dotted line represent the light lines in air and $TiO_2$, respectively. The gray dashed line represents the propagation constant of the GSPP confined in the structure excited by the grating coupled with the normal incident light.

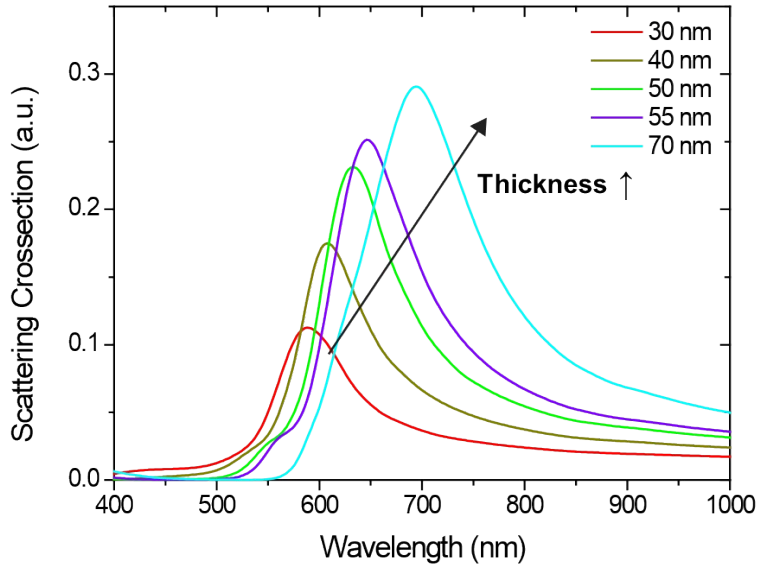


Fig. S6. The FDTD-calculated scattering cross-section spectra of the MDM structure that has a top Au film perforated with a single hole of diameter 220 nm, a middle $TiO_2$ layer and an Au back reflector. The peak position is gradually redshifted with the increase of $TiO_2$ thickness.

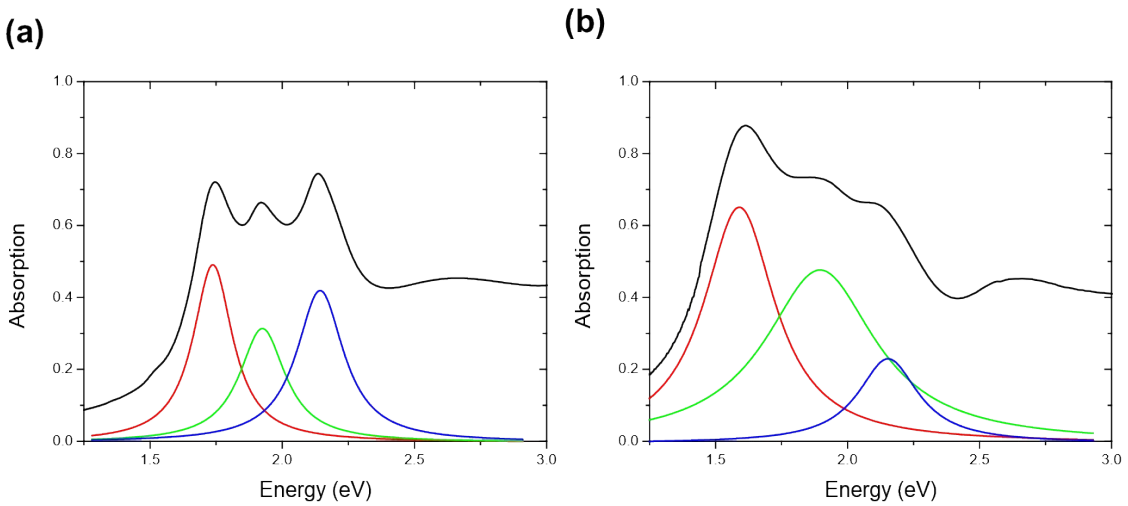


Fig. S7. The FDTD-calculated (a) and experimental (b) absorption spectra of the AuNHA/$TiO_2$/Au MDM absorber with the $TiO_2$ thickness of 55 nm. The color curves represent the Lorentzian fits of the resonances.

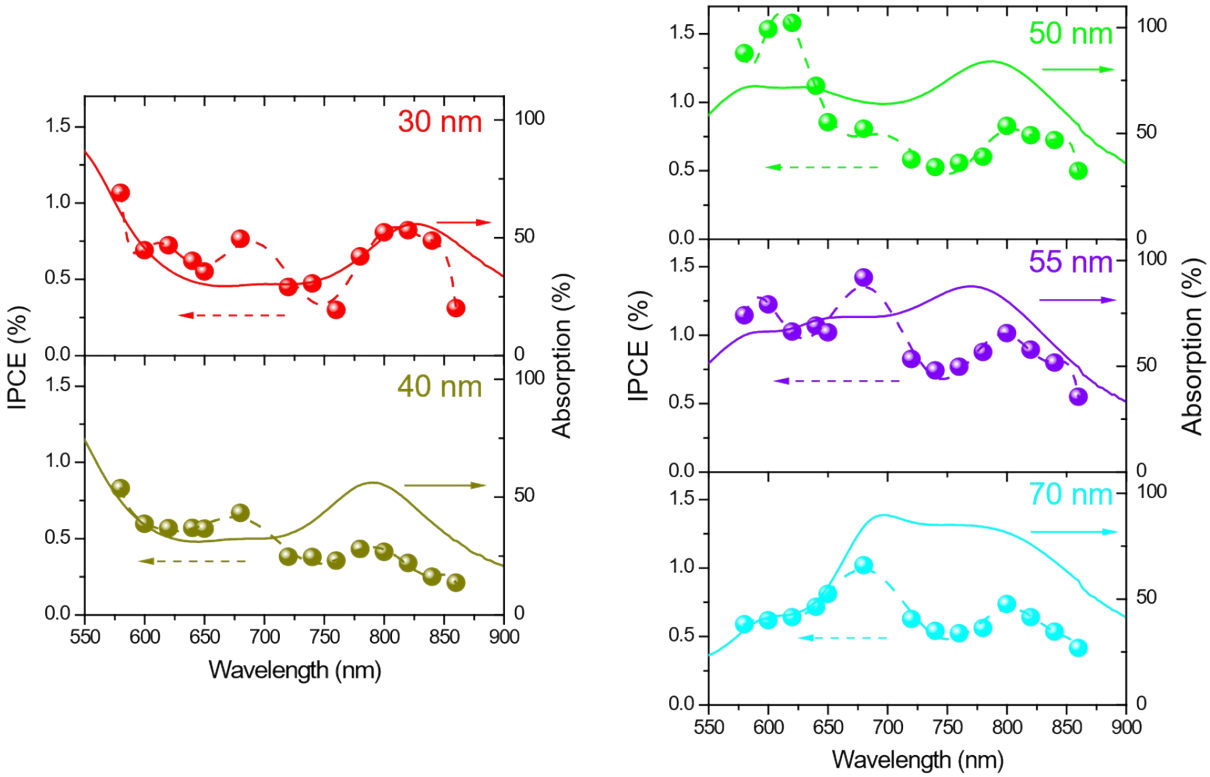


Fig. S8. The IPCE spectra (left axis) and the absorption spectra (right axis) of the MDM structure with varying thickness of $TiO_2$. All the photocurrents generated by the absorbers are measured under the bias voltage of 0.5 V vs. SCE.

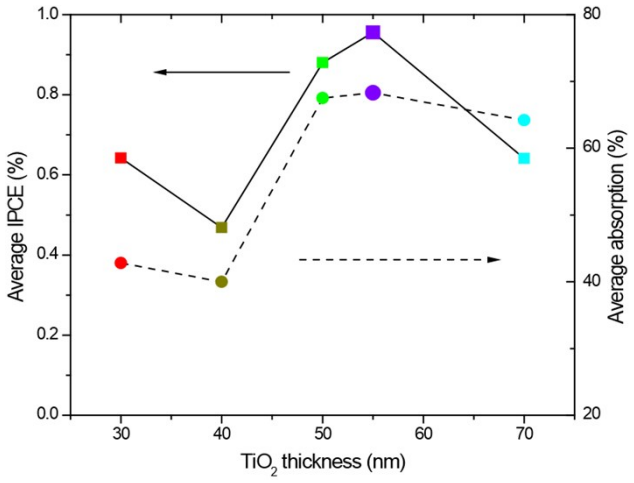


Fig. S9. The average IPCE (left) and the average optical absorption (right) of the MDM absorber with varying thickness of $TiO_2$ over the measurement range from 580 to 860 nm.

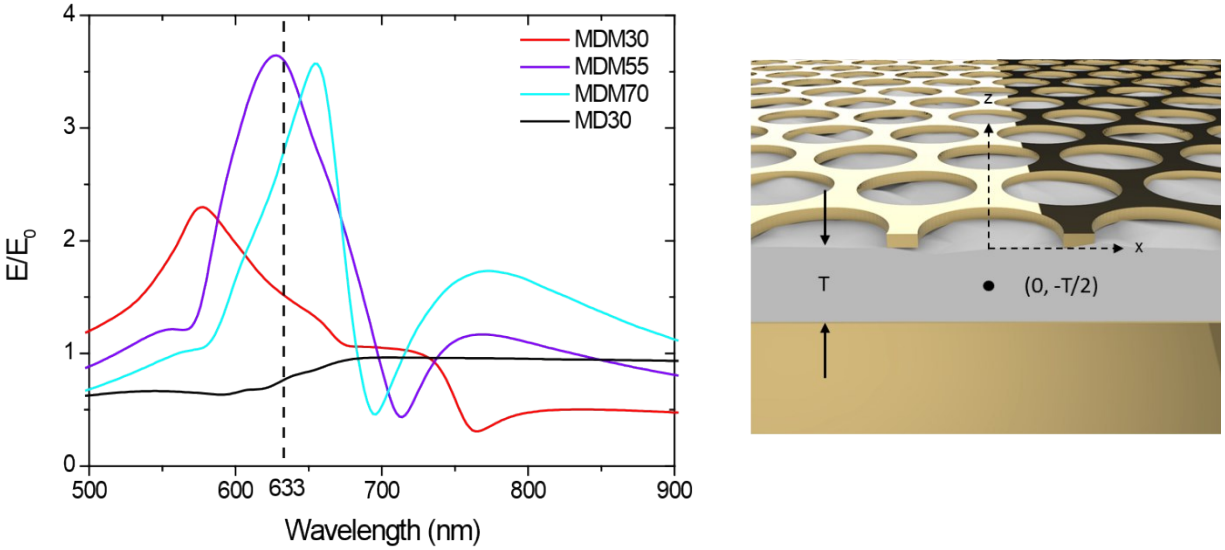


Fig. S10. The FDTD-calculated local electric field spectra of four different structures (i.e., three MDM absorbers with different $TiO_2$ thicknesses and one MD structure without the back reflector). The observation point is located at the middle of the $TiO_2$ below the center of the hole. The dashed line represents the wavelength of the laser source of the SERS.

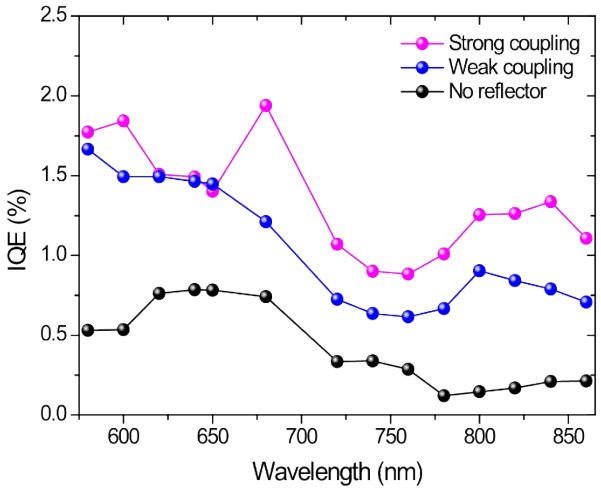


Fig. S11. The interrnal quantum efficiency (IQE) spectra of the MDM structure that fulfills the strong coupllng condtion (magenta), the MDM structure that fail to fulfill the strong coupling condition (blue), and the MD structure that does not support any mode coupling effect (black). The IQE is calculated by deviding the IPCE by the opctical absorption of the absortber.

*Supporting discussion:*

**1. Gap surface plasmon polariton (GSPP) mode**

The dispersion relation of all SPR modes in the system with a dielectric film of thickness *d* sandwiched by two metallic films of thickness h can be implicitly expressed by the following expression [S1, S2]

$$\frac{\left(\frac{k_2}{\varepsilon_{m1}}-\frac{k_3}{\varepsilon_d}\right)\left(\frac{k_1}{\varepsilon_1}+\frac{k_2}{\varepsilon_{m1}}\right)e^{k_2h}e^{-\frac{k_3d}{2}}+\left(\frac{k_2}{\varepsilon_{m1}}-\frac{k_3}{\varepsilon_d}\right)\left(\frac{k_1}{\varepsilon_1}-\frac{k_2}{\varepsilon_{m1}}\right)e^{-k_2h}e^{-\frac{k_3d}{2}}}{\left(\frac{k_2}{\varepsilon_{m1}}+\frac{k_3}{\varepsilon_d}\right)\left(\frac{k_1}{\varepsilon_1}+\frac{k_2}{\varepsilon_{m1}}\right)e^{k_2h}e^{\frac{k_3d}{2}}+\left(\frac{k_2}{\varepsilon_{m1}}-\frac{k_3}{\varepsilon_d}\right)\left(\frac{k_1}{\varepsilon_1}-\frac{k_2}{\varepsilon_{m1}}\right)e^{-k_2h}e^{\frac{k_3d}{2}}}$$
$$-\frac{\left(\frac{k_4}{\varepsilon_{m2}}-\frac{k_3}{\varepsilon_d}\right)\left(\frac{k_5}{\varepsilon_2}-\frac{k_4}{\varepsilon_{m2}}\right)e^{-k_4h}e^{\frac{k_3d}{2}}+\left(\frac{k_4}{\varepsilon_{m2}}+\frac{k_3}{\varepsilon_d}\right)\left(\frac{k_4}{\varepsilon_{m2}}+\frac{k_5}{\varepsilon_2}\right)e^{k_4h}e^{\frac{k_3d}{2}}}{\left(\frac{k_4}{\varepsilon_{m2}}+\frac{k_3}{\varepsilon_d}\right)\left(\frac{k_5}{\varepsilon_2}-\frac{k_4}{\varepsilon_{m2}}\right)e^{-k_4h}e^{-\frac{k_3d}{2}}+\left(\frac{k_4}{\varepsilon_{m2}}-\frac{k_3}{\varepsilon_d}\right)\left(\frac{k_4}{\varepsilon_{m1}}+\frac{k_5}{\varepsilon_2}\right)e^{k_4h}e^{-\frac{k_3d}{2}}}=0 \quad \text{(S1)}$$

where the subscripts 1, 2, 3, 4, and 5 represent the media where the light transmitted sequentially, namely vacuum, Au, $TiO_2$, Au, and $SiO_2$ respectively (schematically shown in fig. S12); $\beta_j$ refers to the propagation constant in medium $j$. The dispersion relations of the internal GSPP mode for different thickness of $TiO_2$ are calculated by the above equation and presented in fig. S5. Of course, the GSPP mode cannot be coupled from free space light without the assistance of a grating or scatterers as the light lines in fig. S5 never cross the dispersion curves. For normal incident light, the GSPP excited by the grating coupling effect provided by an NHA ordered in a hexagonal lattice should obey the conservation of momentum [S3], such that

$$\beta_{GSPP} = \frac{2\pi}{P}\sqrt{\frac{4}{3}(i^2 + i \cdot j + j^2)} \tag{S2}$$

where $P$ is the periodicity of the NHA; $i$ and $j$ are the scattering orders of the NHA. The line associated with lowest grating order, namely (1, 0), is calculated and plotted in fig. S5.

In order to have a better understanding on the GSPP supported by the proposed structure, a structure with only a few holes arranged in the short-range ordered lattice, as shown in fig. S13, are investigated via FDTD. One of the advantages of studying short range ordered structures is the possibility of observing the undisturbed propagating modes. The calculated absorption spectra of the MDM absorbers with 7 holes and 19 holes are presented in fig. S13. For the structures with short range ordered, three peaks which are previously observed in the structure with AuNHA are also discernable at the same spectral positions. The peak with lowest energy for the structure of $TiO_2$ thickness of 55 nm corresponds to the GSPP mode, which the wavelength dependent z-component electric field distribution of the structure at 710 nm can directly identify the GSPP mode propagating in the $TiO_2$ film as positive and negative fields alternatingly distribute along the layer (see fig. S14). Through the time evolution of $E_z$ field shown in fig. S15, it clearly visualizes the propagation of the GSPP mode. For instance, the LSPR mode of the holes are excited at the beginning and then it is coupled to the GSPP which is confined within two metallic films and guided in the $TiO_2$ layer. We further analyze the field

distribution of an arbitrary maximum shown in fig. S14, and plot against the z position (see fig. S16), the symmetric distribution of the field across the AuNHA/$TiO_2$ and $TiO_2$/Au interfaces indicates that the corresponding GSPP mode is a long range guiding mode [S4].

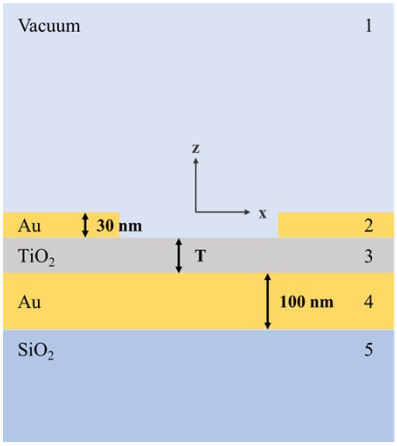


Fig. S12. The schematic diagram of the layer structure in which the calculation in Equation (S1) is implemented.

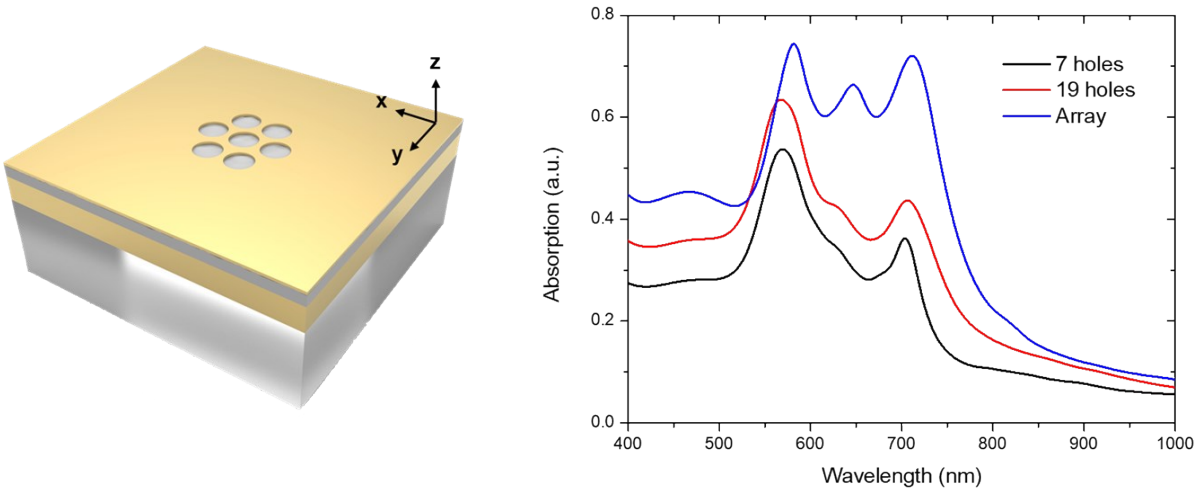


Fig. S13. The schematic diagram of the nonperiodic, hexagonally arranged nanoholes (left) and the corresponding calculated absorption spectra (right). The absorption spectrum of the MDM structure with AuNHA is plotted in the figure (blue curve) for reference.

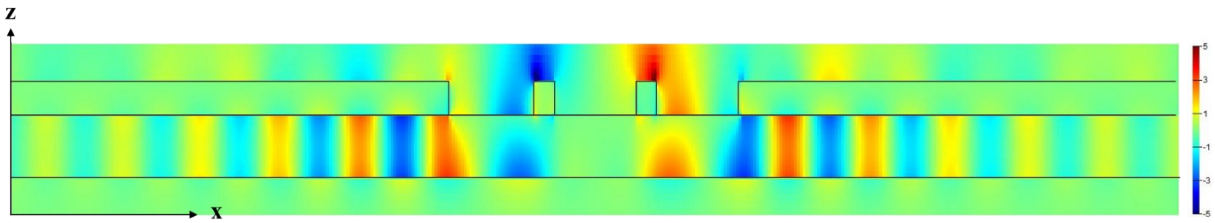


Fig. S14. The $E_z$ distribution of the MDM absorber with 7 nonperiodic nanoholes and $TiO_2$ thickness of 55 nm at the resonance wavelength of 710 nm. The color bar in the diagram from red to green to blue represents the polarity and intensity of the field.

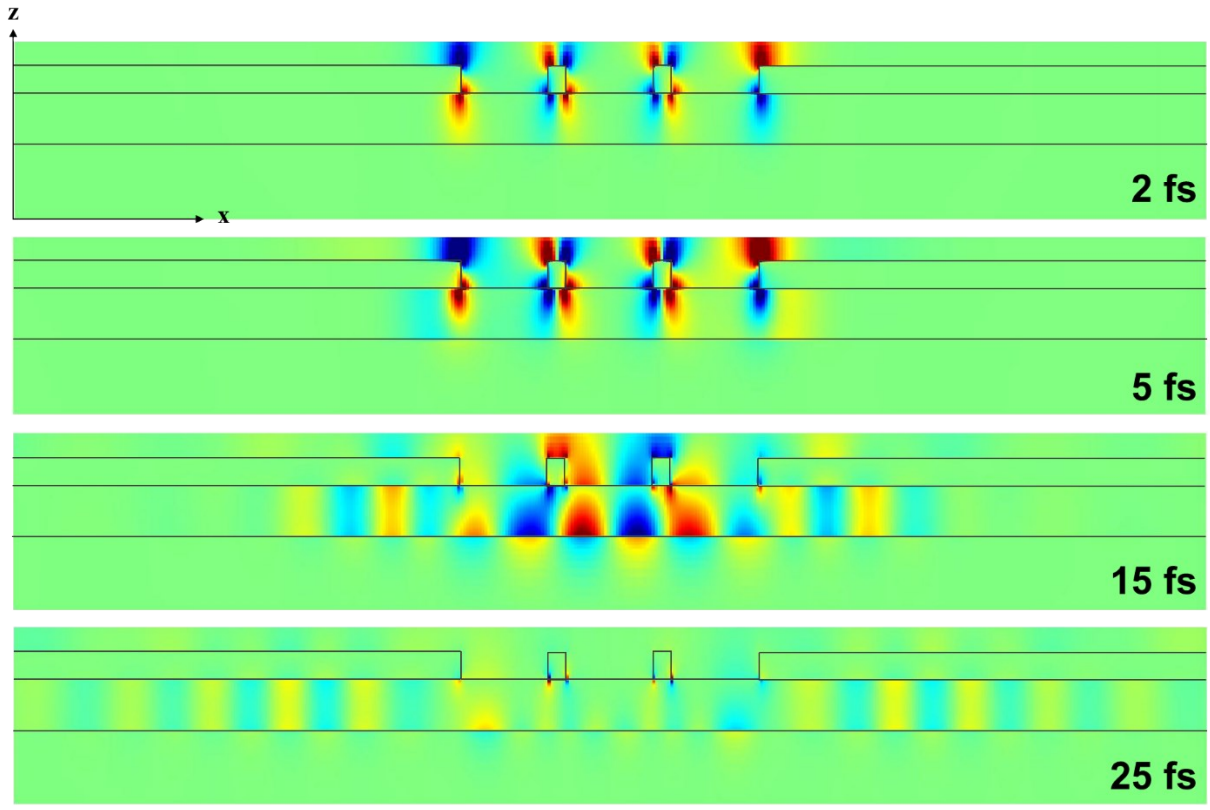


Fig. S15. The time domain $E_z$ field distribution on the xz plane located at y = 0 nm at the time 2, 5, 15, and 25 fs after the start of the simulation. The color in the diagrams represents the same polarity as shown in the color bar in Fig. S14

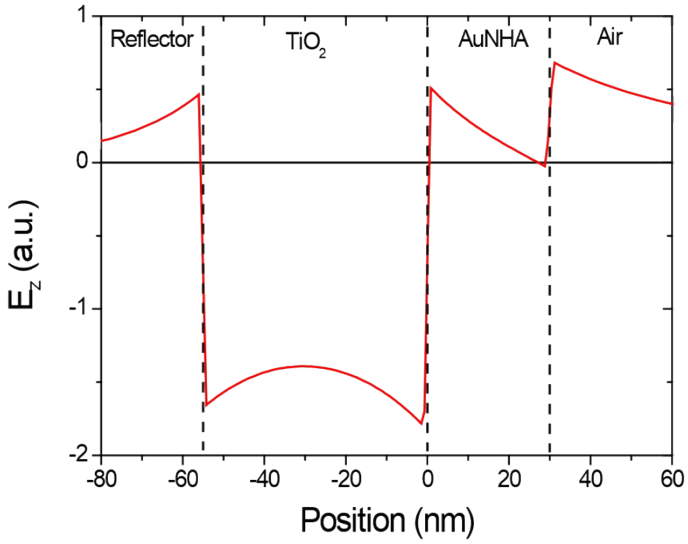


Fig. S16. The intensity of $E_z$ as a function of z position at an arbitrary maximum shown in Fig. S14 at the resonance wavelength of 710 nm.

## References


1. R. Ortuno, C. Garcia-Meca, F. J. Rodriguez-Fortuno, J. Marti and A. Martinez, *Phys. Rev. B*, 2009, **79**.
2. E. Economou, *Phys. Rev.*, 1969, **182**, 539.
3. Q. Li, Z. Li, X. Wang, T. Wang, H. Liu, H. Yang, Y. Gong and J. Gao, *Nanoscale*, 2018, **10**, 19117-19124.
4. P. Berini, *Opt. Exp.*, 2006, **14**, 13030-13042.